

Pseudoscalar production at $\omega\omega$ threshold in $J/\psi \rightarrow \gamma\omega\omega$

M. Ablikim¹, J. Z. Bai¹, Y. Ban¹², J. G. Bian¹, X. Cai¹, H. F. Chen¹⁷, H. S. Chen¹,
 H. X. Chen¹, J. C. Chen¹, Jin Chen¹, Y. B. Chen¹, S. P. Chi², Y. P. Chu¹,
 X. Z. Cui¹, Y. S. Dai¹⁹, L. Y. Diao⁹, Z. Y. Deng¹, Q. F. Dong¹⁵, S. X. Du¹,
 J. Fang¹, S. S. Fang², C. D. Fu¹, C. S. Gao¹, Y. N. Gao¹⁵, S. D. Gu¹, Y. T. Gu⁴,
 Y. N. Guo¹, Y. Q. Guo¹, Z. J. Guo¹⁶, F. A. Harris¹⁶, K. L. He¹, M. He¹³,
 Y. K. Heng¹, H. M. Hu¹, T. Hu¹, G. S. Huang^{1a}, X. T. Huang¹³, X. B. Ji¹,
 X. S. Jiang¹, X. Y. Jiang⁵, J. B. Jiao¹³, D. P. Jin¹, S. Jin¹, Yi Jin⁸, Y. F. Lai¹,
 G. Li², H. B. Li¹, H. H. Li¹, J. Li¹, R. Y. Li¹, S. M. Li¹, W. D. Li¹, W. G. Li¹,
 X. L. Li¹, X. N. Li¹, X. Q. Li¹¹, Y. L. Li⁴, Y. F. Liang¹⁴, H. B. Liao¹, B. J. Liu¹,
 C. X. Liu¹, F. Liu⁶, Fang Liu¹, H. H. Liu¹, H. M. Liu¹, J. Liu¹², J. B. Liu¹,
 J. P. Liu¹⁸, Q. Liu¹, R. G. Liu¹, Z. A. Liu¹, Y. C. Lou⁵, F. Lu¹, G. R. Lu⁵,
 J. G. Lu¹, C. L. Luo¹⁰, F. C. Ma⁹, H. L. Ma¹, L. L. Ma¹, Q. M. Ma¹, X. B. Ma⁵,
 Z. P. Mao¹, X. H. Mo¹, J. Nie¹, S. L. Olsen¹⁶, H. P. Peng^{17b}, R. G. Ping¹, N. D. Qi¹,
 H. Qin¹, J. F. Qiu¹, Z. Y. Ren¹, G. Rong¹, L. Y. Shan¹, L. Shang¹, C. P. Shen¹,
 D. L. Shen¹, X. Y. Shen¹, H. Y. Sheng¹, H. S. Sun¹, J. F. Sun¹, S. S. Sun¹,
 Y. Z. Sun¹, Z. J. Sun¹, Z. Q. Tan⁴, X. Tang¹, G. L. Tong¹, G. S. Varner¹⁶,
 D. Y. Wang¹, L. Wang¹, L. L. Wang¹, L. S. Wang¹, M. Wang¹, P. Wang¹,
 P. L. Wang¹, W. F. Wang^{1c}, Y. F. Wang¹, Z. Wang¹, Z. Y. Wang¹, Zhe Wang¹,
 Zheng Wang², C. L. Wei¹, D. H. Wei¹, N. Wu¹, X. M. Xia¹, X. X. Xie¹, G. F. Xu¹,
 X. P. Xu⁶, Y. Xu¹¹, M. L. Yan¹⁷, H. X. Yang¹, Y. X. Yang³, M. H. Ye², Y. X. Ye¹⁷,
 Z. Y. Yi¹, G. W. Yu¹, C. Z. Yuan¹, J. M. Yuan¹, Y. Yuan¹, S. L. Zang¹, Y. Zeng⁷,
 Yu Zeng¹, B. X. Zhang¹, B. Y. Zhang¹, C. C. Zhang¹, D. H. Zhang¹, H. Q. Zhang¹,
 H. Y. Zhang¹, J. W. Zhang¹, J. Y. Zhang¹, S. H. Zhang¹, X. M. Zhang¹,
 X. Y. Zhang¹³, Yiyun Zhang¹⁴, Z. P. Zhang¹⁷, D. X. Zhao¹, J. W. Zhao¹,
 M. G. Zhao¹, P. P. Zhao¹, W. R. Zhao¹, Z. G. Zhao^{1d}, H. Q. Zheng¹², J. P. Zheng¹,
 Z. P. Zheng¹, L. Zhou¹, N. F. Zhou^{1d}, K. J. Zhu¹, Q. M. Zhu¹, Y. C. Zhu¹,
 Y. S. Zhu¹, Yingchun Zhu^{1b}, Z. A. Zhu¹, B. A. Zhuang¹, X. A. Zhuang¹, B. S. Zou¹

(BES Collaboration)

¹ *Institute of High Energy Physics, Beijing 100049, People's Republic of China*

² *China Center for Advanced Science and Technology(CCAST),
Beijing 100080, People's Republic of China*

³ *Guangxi Normal University, Guilin 541004, People's Republic of China*

⁴ *Guangxi University, Nanning 530004, People's Republic of China*

⁵ *Henan Normal University, Xinxiang 453002, People's Republic of China*

⁶ *Huazhong Normal University, Wuhan 430079, People's Republic of China*

⁷ *Hunan University, Changsha 410082, People's Republic of China*

⁸ *Jinan University, Jinan 250022, People's Republic of China*

⁹ *Liaoning University, Shenyang 110036, People's Republic of China*

¹⁰ *Nanjing Normal University, Nanjing 210097, People's Republic of China*

¹¹ *Nankai University, Tianjin 300071, People's Republic of China*

¹² *Peking University, Beijing 100871, People's Republic of China*

¹³ *Shandong University, Jinan 250100, People's Republic of China*

¹⁴ *Sichuan University, Chengdu 610064, People's Republic of China*

¹⁵ *Tsinghua University, Beijing 100084, People's Republic of China*

¹⁶ *University of Hawaii, Honolulu, HI 96822, USA*

¹⁷ *University of Science and Technology of
China, Hefei 230026, People's Republic of China*

¹⁸ *Wuhan University, Wuhan 430072, People's Republic of China*

¹⁹ *Zhejiang University, Hangzhou 310028, People's Republic of China*

^a *Current address: Purdue University, West Lafayette, IN 47907, USA*

^b *Current address: DESY, D-22607, Hamburg, Germany*

^c *Current address: Laboratoire de l'Accélérateur Linéaire, Orsay, F-91898, France*

^d *Current address: University of Michigan, Ann Arbor, MI 48109, USA*

(Dated: September 7, 2018)

The decay channel $J/\psi \rightarrow \gamma\omega\omega$, $\omega \rightarrow \pi^+\pi^-\pi^0$ is analyzed using a sample of 5.8×10^7 J/ψ events collected with the BESII detector. The $\omega\omega$ invariant mass distribution peaks at 1.76 GeV/ c^2 , just above the $\omega\omega$ threshold. Analysis of angular

correlations indicate that the $\omega\omega$ system below $2 \text{ GeV}/c^2$ is predominantly pseudoscalar. A partial wave analysis confirms the predominant pseudoscalar structure, together with small 0^{++} and 2^{++} contributions, and yields a pseudoscalar mass $M = 1744 \pm 10 \text{ (stat)} \pm 15 \text{ (syst)} \text{ MeV}/c^2$, a width $\Gamma = 244^{+24}_{-21} \text{ (stat)} \pm 25 \text{ (syst)} \text{ MeV}/c^2$, and a product branching fraction $\text{Br}(J/\psi \rightarrow \gamma\eta(1760)) \cdot \text{Br}(\eta(1760) \rightarrow \omega\omega) = (1.98 \pm 0.08 \text{ (stat)} \pm 0.32 \text{ (syst)}) \times 10^{-3}$.

PACS numbers: 12.39.Mk, 13.20.Gd, 13.30.Ce, 14.40.Cs

I. INTRODUCTION

Glueballs are expected to be copiously produced in radiative J/ψ decays. However, until now, no unique experimental signatures of such states have been found. The pseudoscalar ground state mesons (1^1S_0) are well established, and $\pi(1300)$, $\eta(1295)$, $\eta(1475)$, and $K(1460)$ are suggested as the first radial excitations (2^1S_0) of the pseudoscalar mesons [1]. In the Particle Data Group (PDG) listings, two pseudoscalar states are reported in the $\eta(1440)$ mass region. However, there are too many pseudoscalar states, and it is very difficult to find a place for the lower mass $\eta(1440)$ or the $\eta(1760)$ within any $q\bar{q}$ model [1]. At one time, the $\eta(1440)$ was regarded as a glueball candidate when it was observed in J/ψ radiative decay [2] and there was only an upper limit on its two-photon production [3]. But this viewpoint changed when its radiative decay modes [4–7] were observed and it was also observed in untagged $\gamma\gamma$ collisions by the L3 collaboration [8]. In addition, lattice gauge theory would have great difficulty to accommodate such a low-mass 0^{-+} glueball [9].

The $\eta(1760)$ was reported by the MARK III collaboration in J/ψ radiative decays and was found to decay to $\omega\omega$ [10] and $\rho\rho$ [11]. It was also observed by the DM2 collaboration in J/ψ radiative decays in the $\rho\rho$ decay mode with a mass of $M = 1760 \pm 11 \text{ MeV}/c^2$ and a width of $\Gamma = 60 \pm 16 \text{ MeV}/c^2$ [12] and in the $\omega\omega$ decay mode [13]. The BESI experiment reported its $\eta\pi^+\pi^-$ decay with a mass of $M = 1760 \pm 35 \text{ MeV}/c^2$, but without a determination of its width [14]. Also, possible pseudoscalar production at threshold in the $\phi\phi$ mode has been observed in π^-p

scattering [15]. The $\eta(1760)$ was suggested to be a 3^1S_0 pseudoscalar $q\bar{q}$ meson, but some authors suggest a mixture of glueball and $q\bar{q}$ or a hybrid [16, 17]. Recently, in Ref. [18], it was argued that the pseudoscalar glueball may be in the 1.5 to 1.9 GeV/c^2 mass region, and that it also has Vector Vector decay modes. In this paper, we present results from an analysis of $J/\psi \rightarrow \gamma\omega\omega$, $\omega \rightarrow \pi^+\pi^-\pi^0$ decays, based on a sample of 58 million J/ψ events collected with the BESII detector at the Beijing Electron-Positron Collider (BEPC). The presence of a signal around $1.76 \text{ GeV}/c^2$ and its pseudoscalar character are confirmed, and the mass, width, and branching fraction are measured by partial wave analysis.

II. BES DETECTOR AND MONTE CARLO SIMULATION

BESII is a large solid-angle magnetic spectrometer that is described in detail in Ref. [19]. Charged particle momenta are determined with a resolution of $\sigma_p/p = 1.78\%\sqrt{1+p^2}$ (with p in GeV/c) in a 40-layer cylindrical main drift chamber (MDC). Particle identification is accomplished using specific ionization (dE/dx) measurements in the MDC and time-of-flight (TOF) measurements in a barrel-like array of 48 scintillation counters. The dE/dx resolution is $\sigma_{dE/dx} = 8.0\%$; the TOF resolution is $\sigma_{TOF} = 180 \text{ ps}$ for the Bhabha events. Outside of the TOF counters is a 12-radiation-length barrel shower counter (BSC) comprised of gas tubes interleaved with lead sheets. The BSC measures the energies and directions of photons with resolutions of $\sigma_E/E \simeq 21\%/\sqrt{E(\text{GeV})}$, $\sigma_\phi = 7.9 \text{ mrad}$, and $\sigma_z = 2.3 \text{ cm}$. The iron flux return of the magnet is instrumented with three double layers of counters that are used to identify muons.

In this analysis, a GEANT3 based Monte Carlo (MC) simulation program (SIMBES) [20] with detailed consideration of real detector responses (such as dead electronic channels) is used. The consistency between data and Monte Carlo has been carefully checked in many high-purity physics channels, and the agreement is quite reasonable [20].

III. EVENT SELECTION

$J/\psi \rightarrow \gamma + 2(\pi^+\pi^-\pi^0)$ candidates are selected from events with four charged tracks in the drift chamber and five photons in the barrel shower counter.

A. Charged particle identification

Each charged track, reconstructed using MDC information, is required to be well fitted to a helix, to be within the polar angle region $|\cos \theta| < 0.85$, to have a transverse momentum larger than $50 \text{ MeV}/c$, and have the point of closest approach of the track to the beam axis within 2 cm of the beam axis and within 20 cm from the center of the interaction region along the beam line. For each track, we make a weak particle identification requirement: either the TOF or dE/dx information must agree with that expected for a pion within four standard deviations.

B. Photon identification

Each candidate photon is required to have an energy deposit in the BSC greater than 35 MeV , to be isolated from charged tracks by more than 6° , to have the angle between the cluster development direction in the BSC and photon emission direction less than 30° , and to have the first hit in the beginning six radiation lengths.

C. Event selection criteria

Events are required to have four charged tracks with net charge zero and have from 5 to 8 photon candidates. Six-constraint(6-C) kinematic fits to the $J/\psi \rightarrow \gamma + 2(\pi^+\pi^-\pi^0)$ hypothesis are made with both $\gamma\gamma$ invariant masses being constrained to the π^0 mass using all possible photon combinations. Note that there are 15 possible ways of combining five photons to obtain two π^0 s. We select the combination with the highest probability and require this probability to be greater than 10%. Six-constraint kinematic fits also are applied using the $J/\psi \rightarrow 2(\pi^+\pi^-\pi^0)$ hypothesis, and the probability of these fits is required to be less than that of the

signal hypothesis. Two further requirements are imposed on events with more than five gammas to reduce the background from $J/\psi \rightarrow \pi^0 2(\pi^+ \pi^- \pi^0)$. First, all gammas which do not belong to the chosen combination must have $E_\gamma < 140$ MeV. Second, seven-constraint kinematic fits are performed to the $J/\psi \rightarrow \pi^0 2(\pi^+ \pi^- \pi^0)$ hypothesis with the invariant mass of the three $\gamma\gamma$ pairs being constrained to the π^0 mass, and the event is discarded if $P(\chi^2)_{7c} > P(\chi^2)_{6c}$.

The $\pi^+ \pi^- \pi^0$ invariant mass distribution for the selected events is shown in Fig. 1(a), where there are 8 entries per event. A clear ω signal is present, mainly due to $J/\psi \rightarrow \omega \pi^+ \pi^- \pi^0 \pi^0$. The open histogram in Fig. 1(b) shows the $\pi^+ \pi^- \pi^0$ invariant mass spectrum after the requirement that the invariant mass of the other $\pi^+ \pi^- \pi^0$ is inside the ω region ($|m_{\pi^+ \pi^- \pi^0} - m_\omega| < 40$ MeV/ c^2), and the shaded histogram is for events after the requirement that the invariant mass of the other $\pi^+ \pi^- \pi^0$ mass is inside the ω sideband region (40 MeV/ c^2 $< |m_{\pi^+ \pi^- \pi^0} - m_\omega| < 80$ MeV/ c^2).

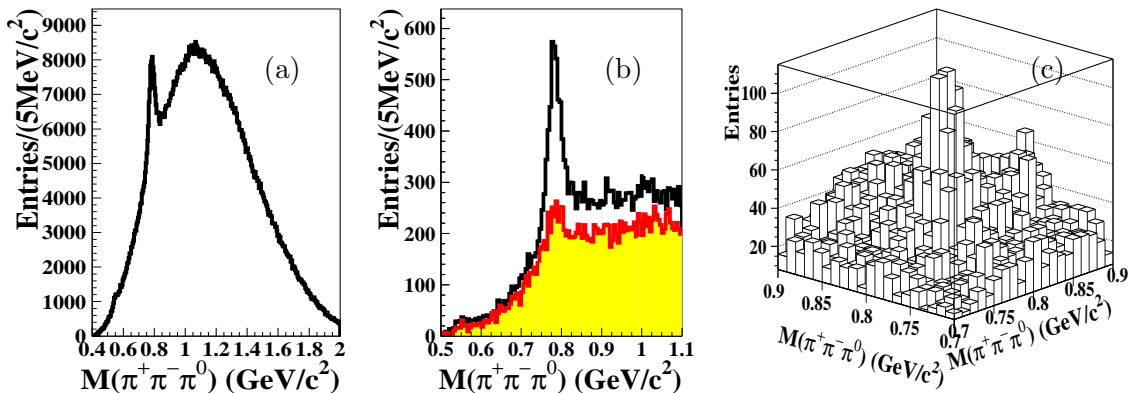


FIG. 1: (a) The $\pi^+ \pi^- \pi^0$ invariant mass distribution (8 entries per event). (b) The $\pi^+ \pi^- \pi^0$ mass distribution for the best $\omega\omega$ combination after the requirement that the invariant mass of the other $\pi^+ \pi^- \pi^0$ is inside the ω region (open histogram), defined by $|m_{\pi^+ \pi^- \pi^0} - m_\omega| < 40$ MeV/ c^2 , or in the sideband range (shaded histogram), defined by 40 MeV/ c^2 $< |m_{\pi^+ \pi^- \pi^0} - m_\omega| < 80$ MeV/ c^2 . (c) The $\pi^+ \pi^- \pi^0$ versus the $\pi^+ \pi^- \pi^0$ invariant mass (4 entries per event).

The $\pi^+ \pi^- \pi^0$ versus $\pi^+ \pi^- \pi^0$ invariant mass distribution (four entries per event) is plotted in Fig. 1(c). A cluster of events is observed corresponding to $\omega\omega$ production. Because the processes $J/\psi \rightarrow \omega\omega$ and $J/\psi \rightarrow \pi^0 \omega\omega$ are forbidden by C-invariance, the presence of two ω 's is direct evidence for the radiative decay $J/\psi \rightarrow \gamma\omega\omega$. The

histogram of Fig. 2(a) shows the $2(\pi^+\pi^-\pi^0)$ invariant mass distribution of events with both $\pi^+\pi^-\pi^0$ masses within the ω range ($|m_{\pi^+\pi^-\pi^0} - m_\omega| < 40 \text{ MeV}/c^2$). There are 3046 events with a clear peak at $1.76 \text{ GeV}/c^2$. The phase space invariant mass distribution and the acceptance versus $\omega\omega$ invariant mass are also shown in the figure. The corresponding Dalitz plot is shown in Fig. 2(b).

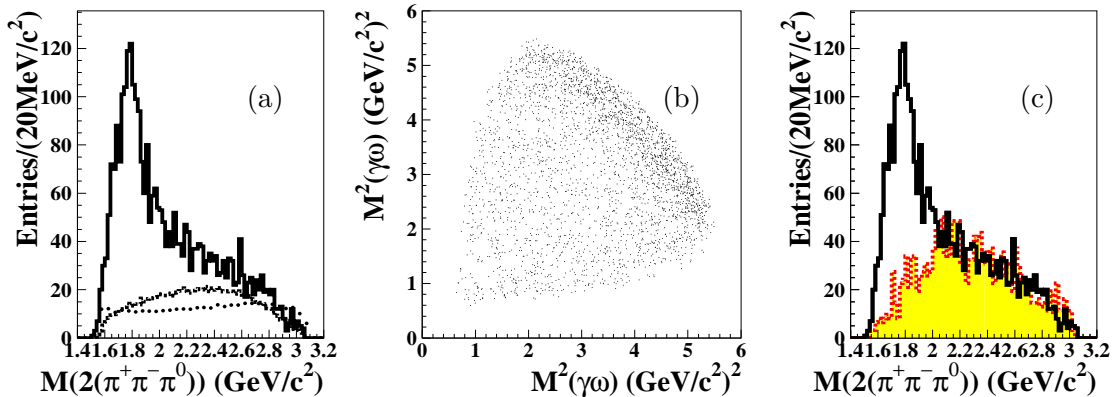


FIG. 2: (a) The $2(\pi^+\pi^-\pi^0)$ invariant mass distribution for candidate events. The dashed curve is the phase space invariant mass distribution, and the dotted curve shows the acceptance versus the $\omega\omega$ invariant mass. (b) The Dalitz plot. (c) The $2(\pi^+\pi^-\pi^0)$ invariant mass of the inclusive Monte Carlo sample (shaded histogram).

From MC simulation, the ω signal can be well fitted with a double Gaussian with widths $14.6 \text{ MeV}/c^2$ and $45.5 \text{ MeV}/c^2$, which makes it difficult to evaluate the background from the sideband events especially for the events near $\omega\omega$ threshold. To ensure that the structure at the $\omega\omega$ mass threshold is not due to background, we have made studies of potential background processes. The main background sources come from $J/\psi \rightarrow \omega\pi^+\pi^-\pi^0\pi^0$, $\gamma 2(\pi^+\pi^-\pi^0)$, and $\pi^0 2(\pi^+\pi^-\pi^0)$. More than one half of the background comes from the first case. However, none of these background channels gives a peak at $1.76 \text{ GeV}/c^2$ in the $2(\pi^+\pi^-\pi^0)$ invariant mass spectrum. In addition, possible backgrounds were checked with a MC sample of 58 million inclusive J/ψ decays generated by the LUND model [21], with $\gamma\omega\omega$ events removed. The shaded histogram of Fig. 2(c) shows the $2(\pi^+\pi^-\pi^0)$ invariant mass distribution of the inclusive sample. There is no peak at the $\omega\omega$ mass threshold in the invariant mass distribution at around $1.76 \text{ GeV}/c^2$, while the inclusive MC distribution is

comparable with data for $2(\pi^+\pi^-\pi^0)$ invariant mass greater than $2 \text{ GeV}/c^2$. A background evaluation is performed by fitting the $\pi^+\pi^-\pi^0$ mass distribution for events with the other $\pi^+\pi^-\pi^0$ within the ω signal region (Fig. 1(b)). The background shape is obtained from the inclusive MC sample, and the signal shape is obtained from the phase space MC sample of $J/\psi \rightarrow \gamma\omega\omega$. The number of events is free in the fitting. The fitting yields 1441 ± 50 background events within the $\omega\omega$ invariant mass range from $1.6 \text{ GeV}/c^2$ to $2.8 \text{ GeV}/c^2$.

IV. ANGULAR CORRELATION ANALYSIS

An analysis of the angular distributions of the accepted events has been performed in order to estimate whether the $\omega\omega$ production below $2 \text{ GeV}/c^2$ belongs to a resonant state with definite spin-parity. Candidate events and side-band background events are analyzed choosing the $\omega\omega$ pair whose quadratic sum of the two differences ($m_{\pi^+\pi^-\pi^0} - m_\omega$) is minimum. For systems of two vector mesons, the distribution of χ , the azimuthal angle between the normals to the two ω decay planes in the $\omega\omega$ rest frame, provides a unique signature for the spin and parity [22–25]. The distribution takes the form $dN/d\chi \propto 1 + \beta \cos(2\chi)$, where β is a constant which is independent of the polarization of the $\omega\omega$ system, but exhibits strong correlation with the spin-parity. β is zero for odd spin and non-zero for even spin. Its sign is the parity of the $\omega\omega$ system. For $J^P = 0^-$, where β is -1 , $dN/d\chi \propto \sin^2 \chi$, and the effect is maximal.

Fig. 3 shows the χ distribution for a) $J/\psi \rightarrow \gamma\omega\omega$ events with $m_{\omega\omega}$ less than $2 \text{ GeV}/c^2$, and b) events from the ω sidebands, where ω sideband is defined with a least one $m_{\pi^+\pi^-\pi^0}$ mass in the range of $40 \text{ MeV}/c^2 < |m_{\pi^+\pi^-\pi^0} - m_\omega| < 120 \text{ MeV}/c^2$. The distributions for signal and background events are strikingly different, indicating a large component with even spin and odd parity in the signal region. The solid line in Fig. 3(a) is the result of a fit to $a + b \sin^2 \chi$, which yields a $\sin^2 \chi$ contribution of the $\gamma\omega\omega$ event candidates below $2 \text{ GeV}/c^2$ of $38.3 \pm 3.5\%$.

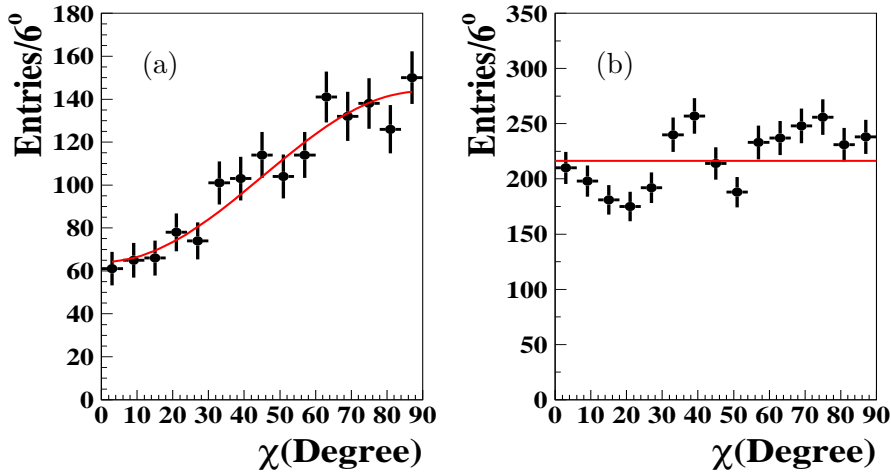


FIG. 3: Distribution of χ , the azimuthal angle between the normals to the two ω decay planes for (a) for $\omega - \omega$ signal events ($m_{\omega\omega} < 2 \text{ GeV}/c^2$) and (b) for ω sideband events ($m_{\omega\omega} < 2 \text{ GeV}/c^2$)

V. PARTIAL WAVE ANALYSIS

A partial wave analysis (PWA) has been carried out for events with $2(\pi^+\pi^-\pi^0)$ invariant mass from $1.6 \text{ GeV}/c^2$ to $2.8 \text{ GeV}/c^2$. The sequential decay process can be described by $J/\psi \rightarrow \gamma X, X \rightarrow \omega\omega$ and $\omega \rightarrow \pi^+\pi^-\pi^0$. The amplitudes of the two body or three body decays are constructed using the covariant helicity coupling amplitude method [26]. The intermediate resonance X is denoted with the normal Breit-Wigner propagator $\text{BW} = 1/(M^2 - s - iM\Gamma)$, where s is the $\omega\omega$ invariant mass-squared and M and Γ are the resonance's mass and width. The amplitude of sequential decay process is the product of all decay amplitudes and the Breit-Wigner propagator.

The χ angular distribution shows a strong contribution from structures with even spin and odd parity for $\omega\omega$ invariant mass below $2 \text{ GeV}/c^2$. Therefore the study of the $\eta(1760)$ is the main goal of this analysis. From the PDG, three f_2 resonances can decay into $\omega\omega$ final states, $f_2(1560)$, $f_2(1640)$, and $f_2(1910)$. Because the mass of $f_2(1560)$ and $f_2(1640)$ are very close, only one resonance, $f_2(1640)$, is considered in the analysis. The $f_0(1710)$ is a well known resonance, and its spin-parity allows it to decay to a $\omega\omega$ final state, so it is included in the fit. Finally, four possible

intermediate resonances $\eta(1760)$, $f_0(1710)$, $f_2(1640)$, and $f_2(1910)$ are included in the final analysis, and the total differential cross section $d\sigma/d\Phi$ is

$$\frac{d\sigma}{d\Phi} = |A(\eta) + A(f_0) + A(f_2^1) + A(f_2^2)|^2 + BG, \quad (1)$$

where $A(\eta)$, $A(f_0)$, $A(f_2^1)$, and $A(f_2^2)$ are the total amplitudes of the resonances $\eta(1760)$, $f_0(1710)$, $f_2(1640)$, and $f_2(1910)$, respectively, and BG denotes the background contribution, which is described by phase space.

The relative magnitudes and phases of the amplitudes are determined by an unbinned maximum likelihood fit. The basis of likelihood fitting is calculating the probability that a hypothesized probability distribution function would produce the data set under consideration. The joint probability density for observing the N events in the data sample is

$$\mathcal{L} = \prod_{i=1}^N P(x_i) \quad (2)$$

where $P(x_i)$ is the probability to produce event i characterized by the measurement x_i , which is the normalized differential cross section:

$$P(x_i) = \frac{\left(\frac{d\sigma}{d\Phi}\right)_i}{\int \frac{d\sigma}{d\Phi} d\Phi} \quad (3)$$

The normalization integral $\int \frac{d\sigma}{d\Phi} d\Phi$ is done by the phase space MC sample, the details are described in Ref. [27]. The free parameters are optimized by MINUIT [28]. Technically, rather than maximizing \mathcal{L} , the $\mathcal{S} = -\ln \mathcal{L}$ is minimized. In the minimization procedure, a change in log likelihood of 0.5 represents a one standard deviation effect for one parameter case.

For the production of a pseudoscalar, only \mathcal{P} waves are allowed in both the radiative decay $J/\psi \rightarrow \gamma X$ and the hadronic decay $X \rightarrow \omega\omega$. For the production of a scalar, both \mathcal{S} and \mathcal{D} waves are possible in both the radiative and hadronic decays, but only \mathcal{S} wave is considered in the fit. For the production of a 2^+ resonance, \mathcal{S} waves in both decays are considered, and two of three \mathcal{D} waves in the radiative decay and only one \mathcal{D} wave in the hadronic decay, corresponding to the lower overall spin of the $\omega\omega$ system, are considered. From the analysis of angular correlations, it is

found that the contributions from $f_0(1710)$, $f_2(1640)$, and $f_2(1910)$ are very small, so the mass and width of these resonances are fixed to PDG values, but the amplitudes are allowed to vary in the fit. The mass and width of the $\eta(1760)$ are obtained from the optimization; the mass and width are $M = 1744 \pm 10 \text{ MeV}/c^2$ and $\Gamma = 244^{+24}_{-21} \text{ MeV}/c^2$, where the errors are statistical. The final global fit, and the contributions of all resonances and backgrounds are shown in Fig. 4.

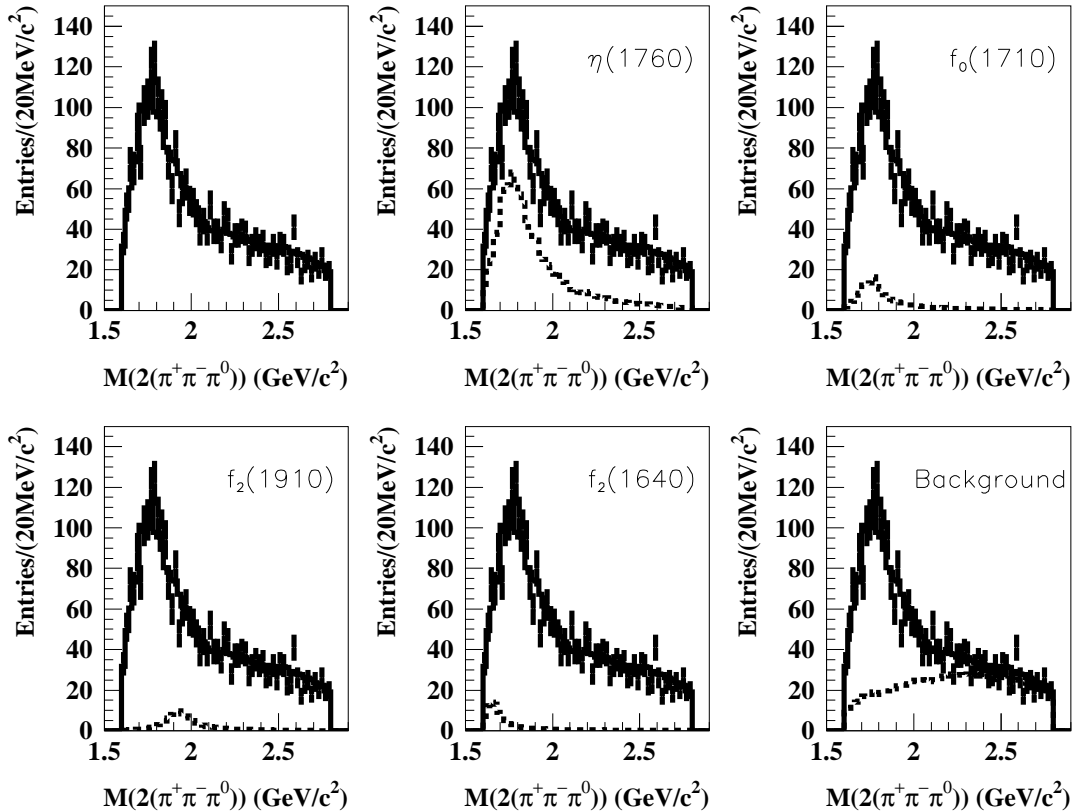


FIG. 4: The $2(\pi^+\pi^-\pi^0)$ invariant mass distribution for $J/\psi \rightarrow \gamma\omega\omega$. The points with error bars are data, the full histograms show the projection of the maximum likelihood fit, and the dashed histograms show the contributions of each of the resonances and background.

Comparisons of angles of fit projections and data are shown in Fig. 5. To determine the goodness of fit, a χ^2 is calculated by comparing the data and fit projection histograms, where χ^2 is defined as [27]:

$$\chi^2 = \sum_{i=1}^N \frac{(n_i - v_i)^2}{v_i} \quad (4)$$

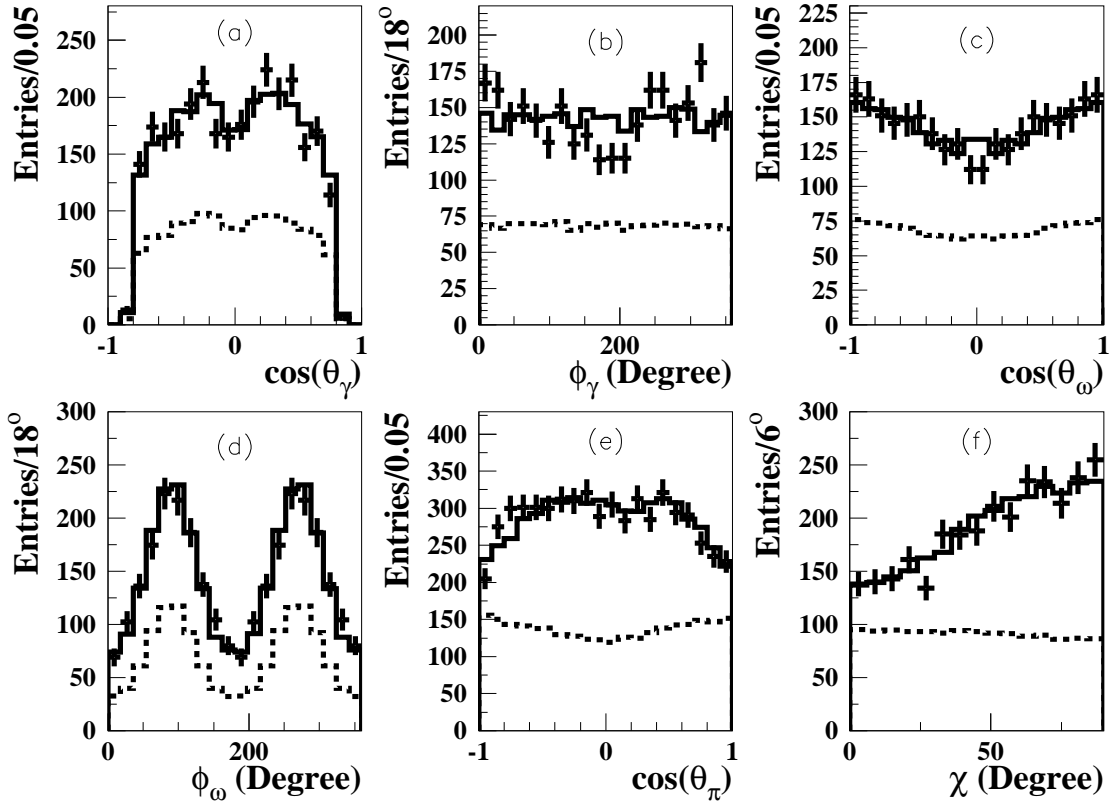


FIG. 5: Comparisons of angular distributions between data and fit projections of the global fit. The dashed histograms show the background contributions. (a, b) The polar and azimuthal angles of the radiative gamma. (c, d) The polar and azimuthal angles of the ω in the $\omega\omega$ rest system. (e) The polar angle of the normal to ω decay plane in the ω rest system, both ω 's angle are projected in the same plot. (f) The χ distribution.

and n_i and v_i are the number of events for data and the fit projections in the i th bin of each figure, respectively. The χ^2 and number of degrees of freedom (ndf) for the $\omega\omega$ invariant mass and the angle distributions are shown in Table I, where the number of bins is taken as the number of degrees of freedom. The values of χ^2/ndf are between 0.6 and 1.8, indicating good agreement between data and the fit.

The numbers of events, detection efficiencies, and the corresponding branching fractions for $J/\psi \rightarrow \gamma X \rightarrow \gamma\omega\omega$ with intermediate resonances $\eta(1760)$, $f_0(1710)$, $f_2(1640)$, and $f_2(1910)$ are shown in the Table II, where the errors are statistical errors only and the correlations between the different resonances are included. The

Variable	mass	θ_γ	ϕ_γ	θ_ω	ϕ_ω	θ_π	χ
χ^2	68.2	20.3	35.2	12.9	14.7	22.5	13.4
<i>ndf</i>	60	18	20	20	20	20	15
χ^2/ndf	1.14	1.13	1.76	0.65	0.74	1.13	0.89
C.L. (%)	21.9	31.6	1.9	88.2	79.3	31.4	57.1

TABLE I: Goodness of fit check for the invariant mass distribution and angular distributions shown in Fig. 5, where *ndf* and C.L. are the number of degrees of freedom and the corresponding confidence level.

magnitudes and phases of the partial amplitudes from the PWA are used in the detection efficiency determination. Details of the fitting procedure and the detection efficiency determination can be found in Ref. [27]. The changes of the log likelihood value $\Delta\mathcal{S}$ when the corresponding resonance is dropped from the fit and the statistical significance for each component are also shown in Table II, where the significance is calculated from the difference between \mathcal{S} values of the fits with and without the resonance. The product branching fraction is $\text{Br}(J/\psi \rightarrow \gamma\eta(1760)) \cdot \text{Br}(\eta(1760) \rightarrow \omega\omega) = (1.98 \pm 0.08 \text{ (stat)}) \times 10^{-3}$, and the statistical significance of the $\eta(1760)$ is above 10σ . All the resonances listed improve the fitting by more than 5σ . If the spin-parity of $\eta(1760)$ is replaced by 0^{++} in the fit, the log likelihood is worse by 248.0, so the possibility that its spin-parity is 0^{++} is excluded by at least 10σ .

The fit determines 1371 ± 45 background events, which is consistent with the result obtained from Fig. 1(b). Another technique for treating background, which was used in Refs. [27, 29, 30], is to set *BG* to 0 in Eq. (1) and to cancel the background contribution by including MC data in the fit with the opposite sign of log likelihood compared to the data. As a check we have also used this method. The MC sample is obtained using the inclusive MC, and the number of background events is fixed to the fitting results of Fig. 1(b). The $\eta(1760)$ mass and width obtained are $1742 \pm 10 \text{ MeV}/c^2$ and $234 \pm 17 \text{ MeV}/c^2$, respectively, and the product branching fraction of $J/\psi \rightarrow \gamma X, X \rightarrow \omega\omega$ is $(2.01 \pm 0.08) \times 10^{-3}$.

resonance	Events	eff(%)	$Br(\times 10^{-3})$	Sys Err(%)	$\Delta\mathcal{S}$	Sig.
$\eta(1760)$	1045 ± 41	1.15	1.98 ± 0.08	16.4	280	$> 10\sigma$
$f_0(1710)$	180 ± 37	1.27	0.31 ± 0.06	25.1	23.5	6.5σ
$f_2(1910)$	151 ± 32	1.68	0.20 ± 0.04	64.9	23.5	5.8σ
$f_2(1640)$	141 ± 26	1.08	0.28 ± 0.05	59.6	21.4	5.5σ

TABLE II: The fitted number of events, detection efficiency, product branching fraction, systematic error, log likelihood value differences, and statistical significance of each resonance.

Other states listed in the PDG between $1.6 \text{ GeV}/c^2$ and $2.0 \text{ GeV}/c^2$, that are consistent with decay into $\omega\omega$ under spin-parity constraints, are the $\eta_2(1645)$, $\eta(1870)$, $f_2(1810)$, $f_2(1950)$. If these resonances are included in the fit, the log likelihood values \mathcal{S} improve by 6.2, 9.0, 8.9, and 8.4, respectively, while the $\eta(1760)$ masses, widths, and branching fractions are consistent with the final fit result within statistical errors. The difference between results including and not including the $\eta(1870)$ will be taken as a systematic error.

The $f_0(1790)$ has been recently claimed in J/ψ decay [29]. If the parameters of $f_0(1710)$ are replaced with those of the $f_0(1790)$, the log likelihood value is improved by 2.8 after the reoptimization. The reoptimized mass, width, and product branching ratio of $\eta(1760)$ are $1744 \pm 10 \text{ MeV}/c^2$, $238 \pm 20 \text{ MeV}/c^2$, and $(1.97 \pm 0.07) \times 10^{-3}$, respectively, and the product branching ratio of f_0 is then $(0.39 \pm 0.07) \times 10^{-3}$ (statistical error only). Recently a scalar enhancement, the $f_0(1812)$, near $\omega\phi$ threshold in $J/\psi \rightarrow \gamma\omega\phi$ decay was reported by the BESII collaboration [31], and information on the corresponding $\omega\omega$ decay mode is very important to understand its nature [32–37]. If the $f_0(1710)$ parameters are replaced with the $f_0(1812)$ [31], the log likelihood value is improved by 0.8 after the reoptimization. The reoptimized mass, width, and product branching ratio of $\eta(1760)$ are $1740 \pm 10 \text{ MeV}/c^2$, $246 \pm 24 \text{ MeV}/c^2$, and $(1.97 \pm 0.07) \times 10^{-3}$, respectively, and the product branching ratio of f_0 is then $(0.26 \pm 0.05) \times 10^{-3}$ (statistical error only). If both the $f_0(1710)$ and $f_0(1812)$ are added in the fitting, the log likelihood values is improved by 5.2. If the $f_0(1710)$'s

parameters are replaced with those of the $f_0(2020)$, the log likelihood value will be improved by 2.9. But if no scalar in this energy region is used in the fit, the log likelihood value is worse by 23.5, corresponding to 6.5σ . From these tests, we conclude that a scalar is needed, but it is very difficult to determine its mass and width accurately due to the dominant contribution of the pseudoscalar. If the parameters of the $f_2(1640)$ are replaced with those of $f_2(1560)$, the likelihood value is improved by 0.55 after mass and width reoptimization. If the parameters of the $f_2(1910)$ are replaced by those of the $f_2(1950)$, the log likelihood value is improved by 2.1. In the final fit, the ω decay amplitude is described with sequential two body decays with \mathcal{P} wave. If the ω decay amplitude is taken to be constant, the results do not change much. In all these tests, the $\eta(1760)$ masses, widths, and the branching fractions are consistent with the final fit results. The differences are included in the systematic errors.

VI. SYSTEMATIC ERROR

The systematic errors are estimated by considering the following: (a) The $f_0(1710)$ is replaced with the $f_0(2020)$. (b) The $f_2(1640)$ is replaced with the $f_2(1560)$. (c) The $f_2(1910)$ is replaced with the $f_2(1950)$. (d) The fit is done with and without the $\eta_2(1870)$. (e) A constant ω amplitude is used in the fit. (f) Different background treatments. (g) Different γ selection criteria: energy greater than 50 MeV/ c^2 , and the minimum angle between the gamma and the nearest charged track greater than 10° . (h) Changing the polar angle requirement of charged tracks to $|\cos\theta| < 0.8$. (i) Changing the 6-C kinematic fit probability requirement from $\text{Prob}_{6c} > 0.1$ to $\text{Prob}_{6c} > 0.05$. (j) Changing the $\pi^+\pi^-\pi^0$ invariant mass requirement from the 40 MeV/ c^2 to 45 MeV/ c^2 . The total errors are obtained by adding the individual errors in quadrature. The total mass and width systematic errors are 0.83% and 10.5%, respectively. For the branching fraction systematic error, the uncertainties in the MDC tracking, the photon identification efficiency, the $\omega \rightarrow \pi^+\pi^-\pi^0$ branching fraction, and the number of J/ψ events are also included, and the total branching fraction systematic errors are 16.4%, 25.1%, 64.9%, and 59.6% for $\eta(1760)$,

$f_0(1710)$, $f_2(1910)$, and $f_2(1640)$, respectively, which are also listed in Table II.

VII. DISCUSSION

The $\eta(1760)$ is prominently produced in $J/\psi \rightarrow \gamma\omega\omega$. Its two-gluon coupling can discriminate between its gluonic and $q\bar{q}$ nature [16, 17]. If perturbative QCD works well and the non-relativistic approximation is applicable, the formalism proposed in Refs. [38, 39], which connects the two-gluon width $\Gamma(\eta(1760) \rightarrow gg)$ of $\eta(1760)$ to the radiative J/ψ branching fraction, $Br(J/\psi \rightarrow \gamma\eta(1760))$, can be used (see Ref. [38], Eq. 3.4):

$$10^3 Br(J/\psi \rightarrow \gamma\eta(1760)) = \left(\frac{M}{1.5 \text{ GeV}/c^2} \right) \left(\frac{\Gamma_{\eta(1760) \rightarrow gg}}{50 \text{ MeV}/c^2} \right) \frac{x|H_{ps}(x)|^2}{45}, \quad (5)$$

where M is the $\eta(1760)$ mass, $\Gamma_{\eta(1760) \rightarrow gg}$ is the width to gg , and $x|H_{ps}(x)|^2$ is the magnitude of the loop integral calculated in Ref. [38]. Therefore, the gluonic content of $\eta(1760)$ is estimated by its two-gluon coupling, which is calculated from its mass, width, and branching fraction in J/ψ radiative decay. Rewriting $\Gamma_{\eta(1760) \rightarrow gg}$ as $\Gamma_{\eta(1760)} \cdot Br(\eta(1760) \rightarrow gg)$ and multiplying both sides of the equation by $Br(\eta(1760) \rightarrow \omega\omega)$, we obtain:

$$\begin{aligned} & Br(\eta(1760) \rightarrow gg) \cdot Br(\eta(1760) \rightarrow \omega\omega) \\ &= 10^3 [Br(J/\psi \rightarrow \gamma\eta(1760)) \cdot Br(\eta(1760) \rightarrow \omega\omega)] \left(\frac{1.5 \text{ GeV}/c^2}{M} \right) \left(\frac{50 \text{ MeV}/c^2}{\Gamma_{\eta(1760)}} \right) \frac{45}{39} \\ &\simeq \frac{98 \pm 16 \text{ MeV}}{244^{+35}_{-33} \text{ MeV}} = 0.40^{+0.08}_{-0.09}, \end{aligned}$$

where $x|H_{PS}(x)|^2$ is taken as 39, which is obtained from Fig.1 of Ref. [38], and the theoretical uncertainty is not considered. Since we expect $Br(\eta(1760) \rightarrow \omega\omega) < 1.0$, the relationship above implies $Br(\eta(1760) \rightarrow gg) > 0.28$ at 90% confidence level.

From a theoretical viewpoint, the coupling of a glueball to two photons is expected to be very weak, so the study of $\eta(1760)$ production in the two photon process is needed. The $\eta(1760)$ is abundantly produced in the J/ψ radiative decay, but it is not seen in $J/\psi \rightarrow \gamma\gamma V(\rho, \phi)$ [4–7], which means that the partial width of $\eta(1760) \rightarrow \gamma V(\rho, \phi)$ is very small. $\eta(1760)$ is shown to have large gluon component,

but its mass is much lower than the prediction from lattice QCD calculation [9], suggesting that it is a mixture of the glueball and $q\bar{q}$ meson. If $\eta(1760)$ is a mixed pseudoscalar glueball candidate, it should have flavor symmetric decays. Therefore other decay modes of $\eta(1760)$, such as $\eta(1760) \rightarrow \rho\rho$, K^*K^* , $\eta\pi\pi$, $K\bar{K}\pi$, etc. should be studied. Further studies are needed to understand the nature of the $\eta(1760)$, both experimentally and theoretically.

VIII. SUMMARY

In summary, $J/\psi \rightarrow \gamma\omega\omega$, $\omega \rightarrow \pi^+\pi^-\pi^0$ is studied, and the $\omega\omega$ invariant mass distribution peaks at $1.76 \text{ GeV}/c^2$. The partial wave analysis shows that the structure is predominantly pseudoscalar, with small contributions from $f_0(1710)$, $f_2(1640)$, and $f_2(1910)$. The mass of the pseudoscalar is $M = 1744 \pm 10 \text{ (stat)} \pm 15 \text{ (syst)} \text{ MeV}/c^2$, the width $\Gamma = 244^{+24}_{-21} \text{ (stat)} \pm 25 \text{ (syst)} \text{ MeV}/c^2$, and the product branching fraction is $\text{Br}(J/\psi \rightarrow \gamma\eta(1760)) \cdot \text{Br}(\eta(1760) \rightarrow \omega\omega) = (1.98 \pm 0.08 \text{ (stat)} \pm 0.32 \text{ (syst)}) \times 10^{-3}$. The corresponding product branching fractions with intermediate resonances $f_0(1710)$, $f_2(1640)$, and $f_2(1910)$ are also determined, but with larger errors.

IX. ACKNOWLEDGMENT

The BES collaboration thanks the staff of BEPC and computing center for their hard efforts. This work is supported in part by the National Natural Science Foundation of China under contracts Nos. 10491300, 10225524, 10225525, 10425523, the Chinese Academy of Sciences under contract No. KJ 95T-03, the 100 Talents Program of CAS under Contract Nos. U-11, U-24, U-25, and the Knowledge Innovation Project of CAS under Contract Nos. U-602, U-34 (IHEP), the National Natural Science Foundation of China under Contract No. 10225522 (Tsinghua University), and the Department of Energy under Contract No. DE-FG02-04ER41291 (U Hawaii).

[1] Particle Data Group, S. Eidelman et al., Phys. Lett. B **592**, 1 (2004).

- [2] D. L. Scharre et al., Phys. Lett. B **97**, 329 (1980).
- [3] H. J. Behrend et al. (CELLO Collaboration), Z. Phys. C **42**, 367 (1989).
- [4] D. Coffman et al. (MARK-III Collaboration), Phys. Rev. D **41**, 1410 (1990).
- [5] J. E. Augustin et al. (DM2 Collaboration), Phys. Rev. D **42**, 10 (1990).
- [6] C. Edwards, PhD thesis, Cal. Tech. Preprint CALT-68-1165 (1985).
- [7] M. Ablikim et al. (BES Collaboration), Phys. Lett. B **594**, 47 (2004).
- [8] I. Vodopianov (L3 Collaboration), Acta Phys. Polon. B **31**, 2453 (2000).
- [9] C. J. Morningstar and M. Peardon, Phys. Rev. D **60**, 034509 (1999).
- [10] R. M. Baltrusaitis et al. (MARKIII Collaboration), Phys. Rev. Lett. **55**, 1723 (1985).
- [11] R. M. Baltrusaitis et al. (MARKIII Collaboration), Phys. Rev. D **33**, 1222 (1986).
- [12] D. Bisello et al. (DM2 Collaboration), Phys. Rev. D **39**, 701 (1989).
- [13] D. Bisello et al. (DM2 Collaboration), Phys. Lett. B **192**, 239 (1987).
- [14] J. Z. Bai et al. (BES Collaboration), Phys. Lett. B **446**, 356 (1999).
- [15] A. Etkin et al., Phys. Rev. Lett. **40**, 422 (1978).
- [16] P. R. Page, X. Q. Li, Eur. Phys. J. C1, **579** (1998).
- [17] N. Wu et al, Chin. Phys. **10**, 611 (2001); /hep-ph/0011338.
- [18] B. A. Li, hep-ph/0510093 (2005).
- [19] J. Z. Bai et al. (BES Collaboration), Nucl. Instr. Meth. A **344**, 319 (1994).
- [20] M. Ablikim et al. (BES Collaboration), Nucl. Instr. Meth. A **552**, 344 (2005)
- [21] J. C. Chen et al., Phys. Rev. D **62**, 034003 (2000).
- [22] N. P. Chang and C. A. Nelson, Phys. Rev. Lett. **40**, 1617 (1978).
- [23] T. L. Trueman et al., Phys. Rev. D **18**, 3423 (1978).
- [24] R. M. Baltrusaitis et al., Phys. Rev. Lett. **52**, 2126 (1984).
- [25] D. Bisello et al. (DM2 collaboration), Nucl. Phys. B **350**, 1 (1991).
- [26] N. Wu and T. N. Ruan, Commun. theor. Phys. (Beijing, China) **35**, 547 (2001); **35**, 693 (2001); **37**, 309 (2002).
- [27] M. Ablikim et al. (BES Collaboration), Phys. Rev. D **72**, 092002 (2005).
- [28] CERN Program Library D **506**.
- [29] M. Ablikim et al. (BES Collaboration), Phys. Lett. B **610**, 192 (2005) .
- [30] M. Ablikim et al. (BES Collaboration), Phys. Lett. B **598**, 149 (2004).

- [31] M. Ablikim et al. (BES Collaboration), Phys. Rev. Lett. **96**, 162002(2006).
- [32] B. A. Li, hep-ph/0602072.
- [33] P. Bicudo et al., hep-ph/0602172.
- [34] K. T. Chao, hep-ph/0602190.
- [35] D.V. Bugg, hep-ph/0603018.
- [36] Xiao-Gang He, Xue-Qian Li et al., Phys. Rev. D **73**, 051502 (2006).
- [37] Xiao-Gang He, Xue-Qian Li et al., hep-ph/0604141.
- [38] F. E. Close, G. R. Farrar, Z. Li, Phys. Rev. D **55**, 5749 (1997).
- [39] M. B. Cakir, G. R. Farrar, Phys. Rev. D **50**, 3268 (1994).